The Impact of Glacial Suspension Color on the Relationship Between Its Properties and Marine Water Spectral Reflectance

Kornelia Anna Wójcik-Długoborska, Maria Osińska, and Robert Józef Bialik

***Abstract*—This study enabled us to determine the sources of sediment for glacial catchments and investigate the differences in properties, i.e., suspended sediment concentration (SSC), turbidity measured in the laboratory (T_{LAB}) and in the field (T_F), mean particle diameter (MPD), and chemical composition, between two different-colored sediments that flowed from the glacier terminus. Additionally, the relationship between these properties for two types of suspensions and remote sensing reflectance (R_{RS}) was tested, and the factor with the greatest impact on the value of R_{RS} was determined. The results showed that within one catchment area, there were four sediment sources that provide white (S.1) and red (S.2) sediment. Chemical analysis showed that the differences in sediment color may be influenced by the increased content of carbonates in the white sediment (S.1). The S.2 sediment is characterized by mean T_{LAB}, T_F, and SSC values higher than 26.6 formazine nephelometric units (FNU), 13.5 FNU, and 50 mg/L, respectively, and the mean MPD was 4.25 lower than that of the S.1 sediment. However, the red sediment had on average 0.1 lower R_{RS} than the white sediment. In addition, the properties of S.1 correlated better with reflectance, reaching a maximum correlation of 0.69 (SSC/R_{RS} 770–810 nm), while S.2 exhibited a negative correlation in 7 out of 12 cases, reaching a maximum correlation of 0.16 (T_{LAB}/SSC/R_{RS} 730–740 nm) and a negative correlation of −0.37 (SSC/R_{RS} 530–570 nm). This result indicated that sediment color may be a key factor in the dependence of glacial suspension properties and spectral reflectance.**

***Index Terms*—Ocean color, ocean turbidity, optical remote sensing.**

I. Introduction

OPTICAL remote sensing has been utilized to try and meet the challenge posed by intensive environmental changes for a long time. Due to the development of local and global algorithms [1], which, based on remote-acquired imageries, both digital and spectral, quantitative information about the parameters of water suspension could be provided [2], [3]. Nevertheless, these algorithms mainly concern areas of high economic interest [4]. However, the specificity of the polar regions is different. Retreating tidewater glaciers reveal new shallow and small bays [5], [6]. As a result of the increasingly intense melting of glaciers, diversified sediment results from the uneven geological structure of the substrate. This material can be delivered to shallow coves and fjords in different ways and can come from a variety of sources, both from the surface and glacial runoff, and this causes variations in particle size and concentration and the chemical and mineral composition of the suspension [7], [8]. These components of suspension can have a significant impact on optical properties and, in effect, on water color, which is a primary indicator for the application of ocean color radiometry (OCR) [3]. In summary, glacial suspensions can be very diverse, and the created OCR algorithms, despite enormous efforts, are unable to take into account all the variables affecting the amount of reflectance, such as grain size and shape, sediment color and mineral characteristics of the sediment particles, turbidity, and concentration [9]–[11].

To investigate the dependence of the factors influencing the amount of reflectance in the polar maritime environment for two different colored sediments provided to one glacial cove, a twofold goal was set in this article: The first goal was to determine the sources of sediment for this glacial catchment and investigate the differences in properties, i.e., suspended sediment concentration (SSC), turbidity measured in the laboratory (T_{LAB}) and in the field (T_F), mean particle diameter (MPD), and chemical composition, between two different colored sediments that flowed from one glacier terminus. The second goal was to examine the interrelationship between these parameters for two types of suspensions and the remote sensing reflectance (R_{RS}) and determine which factor has the greatest impact on the value of R_{RS}. Moreover, we hypothesized that in the polar regions, the amount of radiation reflection depends more on the color of the suspension resulting from the chemical composition than on the quantitative parameters; therefore, the relationship between the parameters and reflection will be different for different types of sediment. In this article, we present the first such extensive research on the use of drones (with both spectral and RGB cameras) and *in situ* research on intensively forming various plumes in the area of the newly exposed cove near the

Manuscript received December 24, 2021; revised March 11, 2022; accepted March 30, 2022. Date of publication April 11, 2022; date of current version May 6, 2022. This work was supported in part by the National Science Centre, Poland, under Grant 2017/25/B/ST10/02092 "Quantitative Assessment of Sediment Transport from Glaciers of South Shetland Islands on the Basis of Selected Remote Sensing Methods" and in part by the Institute of Biochemistry and Biophysics PAS, under Grant SBM-17/21. *(Corresponding author: Robert Józef Bialik.)*

Kornelia Anna Wójcik-Długoborska and Robert Józef Bialik are with the Institute of Biochemistry and Biophysics, Polish Academy of Sciences, 02-106 Warsaw, Poland (e-mail: kwojcik@ibb.waw.pl; rbialik@ibb.waw.pl).

Maria Osińska is with the Institute of Oceanography, University of Gdańsk, 81-378 Gdynia, Poland (e-mail: maria.osinska@phdstud.ug.edu.pl).

Digital Object Identifier 10.1109/JSTARS.2022.3166398

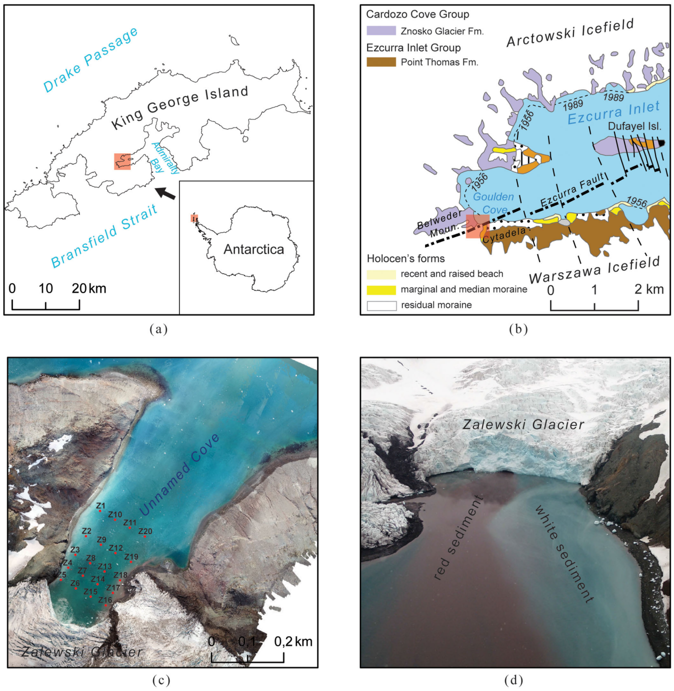

Fig. 1. Research area. (a) Antarctica and King George Island. (b) Geological map [15]. (c) Zalewski Glacier and measurement points. (d) Two types of sediment supplied from glaciers.

Zalewski Glacier terminus in Antarctica. By virtue of a long series of measurements and the fusion of advanced UAV spectral technology and field measurements, it was possible to observe the glacier's activity in time and the presence of two plumes of different colors on the surface and study their physicochemical parameters and spectral properties.

II. Materials and Methods

A. Research Area

Fig. 1(a) shows an unnamed cove near the Zalewski Glacier on King George Island in the South Shetland archipelago, approximately 100 km from the West Antarctic Peninsula, where this research was conducted. This tidewater glacier's active front elevation reaches 33 m, and the active front width is 445 m. The Cove area is 0.19 km^2, and the cove coast length is 1662 m [12]. The mean depth of the cove is 17.31 m, and the maximum depth reaches 41 m [13]. Zalewski Glacier is located directly over the Ezcurra Fault, dividing the rocks that build the glacier catchment area into two geologically different groups as illustrated in Fig. 1(b) [14]. Zalewski Glacier and measurement points are presented in Fig. 1(c).

The rocks of Belweder Mountain lie directly at the base of the glacier, north of the fault, belong to the Znosko Glacier Formation, which is part of the Barton Horst tectonic complex and mainly consists of green, basic andesite lavas alternating with tuff and agglomerate, sometimes with petrified wood fragments. The rocks were subject to strong metasomatic changes (chloritization and carbonatization), and dating indicates a Paleocene age of this formation [15]. To the south (Cytadela) of the fault are

TABLE I
Measurements Performed, Their Specifications, and the Type of Sediment Observed

Date	Hour	Type of measurement	GSD [cm]		Type of sediment (based on UAV images)
			Inspire 2	Parrot	
11.12.2019	11 a.m.-1 p.m.	Inspire/*in situ*	2.94	-	white/red
20.12.2019	8-9 a.m.	*In situ*	-		-
30.12.2019	2-3 p.m.	Inspire/*in situ*	2.96	-	white/red
04.01.2020	7-8 p.m.	Inspire/*in situ*	2.93	-	white/red
09.01.2020	6:30-8 a.m.	Inspire/Parrot/*in situ*	2.89	15.11	white/red
17.01.2020	6:30-8 a.m.	Inspire/Parrot/*in situ*	3.06	14.91	white
27.01.2020	8:30-10:50 a.m.	Inspire/Parrot/*in situ*	3.10	14.90	white
02.02.2020	1:30-2:15 p.m.	*in situ*	-		-
04.02.2020	06:30-08:20 a.m.	Inspire/Parrot/*in situ*	2.99	15.08	white
08.02.2020	10:00-11 a.m.	Inspire/Parrot/*in situ*		15.02	white
18.02.2020	07:30 a.m.-2 p.m.	Inspire/Parrot/*in situ*	3.05	14.97	white
20.02.2020	2:40-3:30 p.m.	*In situ*	-		-
28.02.2020	10-10:35 a.m.	*In situ*	-		-
07.03.2020	4-5:40 p.m.	Inspire/Parrot/*in situ*		14.88	white/red/shadow
09.03.2020	3-5 p.m.	Inspire/Parrot/*in situ*	3.01	15.40	white/red/shadow
19.03.2020	11 a.m.-1 p.m.	Inspire/*in situ*	2.92	-	white
23.03.2020	2-2:10 p.m.	Inspire		-	white
06.04.2020	10-12 a.m.	Inspire/*in situ*	2.96	-	white
22.04.2020	12:30-12:40 p.m.	Inspire		-	Sea Ice
05.05.2020	1:40-2:50 p.m.	Inspire/Parrot/*in situ*	2.92	14.83	white/red
10.05.2020	12:40-12:50 p.m.	Inspire		-	white
24.05.2020	1:30-3:10 p.m.	Inspire/*in situ*		-	white
01.07.2020	12:40-2 p.m.	Inspire/Parrot/*in situ*	2.97	14.16	invisible
23.07.2020	11 a.m.-12:30 p.m.	Inspire/*in situ*	3.00	-	invisible
07.08.2020	1-2 p.m.	Inspire/*in situ*	2.97	-	invisible
16.11.2020	2-3 p.m.	Inspire/*in situ*	3.06	-	white/red
25.11.2020	10:20-11:20 a.m.	Parrot/*in situ*	-	0.41	white/red
02.12.2020	11-12 a.m.	Inspire/*in situ*	2.96	-	white
04.12.2020	1:20-3:10 p.m.	Inspire/*in situ*	2.91	-	white/red
12.12.2020	15-16:10 p.m.	Inspire		-	white/red/shadow
14.12.2020	12-1:05 p.m.	Inspire/Parrot/*in situ*	2.98	14.76	white/red
18.12.2020	12:30-1:35 p.m.	Inspire/Parrot/*in situ*	3.00	15.12	white/red
27.12.2020	6:35-8:15 p.m.	Inspire/*in situ*	2.92	-	white/red
06.01.2021	6:15-8 p.m.	Inspire/*in situ*	2.98	-	white/red
12.01.2021	8:50-10:05 a.m.	Inspire/Parrot/*in situ*	2.95	14.89	white/red
19.01.2021	10:25-11:30 a.m.	Inspire/Parrot/*in situ*	3.10	14.80	white/red
02.02.2021	2:45-3:20 p.m.	Parrot/*in situ*	-	15.32	white/red
17.02.2021	8:40-9:10 a.m.	Parrot/*in situ*	-	15.13	white/red
20.02.2021	4:15-4:50 p.m.	*in situ*	-		-
23.02.2021	4:50-5:30 p.m.	Parrot/*in situ*	-	14.85	white/red

the Point Thomas Formation rocks, which are part of the Ezcurra Inlet Group. This formation comprises flow basalts alternating with pyroclastics at the base, followed by lenticular basalt lavas, feldsparphyric tuffs, and coarse vent brecias with subordinate plant-bearing tuffs. The age of the rocks is determined from the Uppermost Eocene to Lower Oligocene [15]. The glacier, as a result of glacial runoff, provides both types of sediment that form the sedplume on the surface of the cove as shown in Fig. 1(d) [12].

B. UAV Images and Postprocessing

Overflights were carried out by two drones: the DJI Inspire 2 quadcopter with a Zenmuse X5S camera (RGB system) and the Parrot Bluegrass with a Sequoia+ sensor. To register the shape and color of the plumes on the cove's surface, DJI Inspire 2 flights were undertaken first. By using a high-resolution Zenmuse camera taking 30 frames per second and 16-megapixel imagery, with lens FOV 72° (MFT 15 mm/1.7 ASPH), it was possible to obtain images with a pixel resolution from 2.89 to 3.10 cm (see Table I). Then, the amount of radiation reflected from the water surface was recorded with a Sequoia+ spectral camera, which records the image in four spectral bands – green (530–570 nm), red (640–680 nm), red edge (RE) (730–740 nm), and near-infrared (NIR) (770–810 nm) wavelengths. Details about drone specifications and the methodology of the flights are outlined in [12].

TABLE II
RESULTS OF THE CLASSIFICATION OF MEASURING POINTS TO THE INDIVIDUAL SEDIMENT TYPES

Number of measured points	Sediment type			
	White - S.1	Red – S.2	Composite zone	Zone <4 FNU
All points	272	92	46	53
Taken for analysis:				
MPD	256	69	-	-
T_{LAB}	272	92	-	-
T_F	272	92	-	-
SSC	272	92	-	-

Orthophotos and R_{RS} maps were created using Pix4D software. To output the orthomosaic in the WGS1984 UTM Zone 21S, a 3D map template was used. The program matched images and generated a point cloud from which the orthomosaics were created. Default settings were used that gave favorable results. Using UAV multispectral imagery and the AgMultispectral template (Pix4D), R_{RS} maps were created. The Parrot Sequoia+ camera has two calibration modes. The first mode is based on two sensors: one sensor is a fully integrated sunshine sensor that logs light conditions and measures the amount of downward radiation during flights, and the second sensor is a spectral sensor that registers the amount of upward radiation. Based on these measurements, the camera carries self-calibration. The second mode uses external calibration targets. Due to the erroneous spectral reflectance results for some flights that were obtained during the application of additional calibration using external calibration targets, R_{RS} maps were created only on the basis of self-calibration.

To obtain the dominant sediment color on the water surface on orthophotos, the maximum RGB algorithm was applied [16]. To match the maximal/minimal intensity of the channel for every pixel, RGB values were used. Initially, the maximum of the R, G, and B values [$m = \max(R, G, B)$] was determined. If $R < m$, then $R = 0$. If $G < m$, then $G = 0$. If $B < m$, then $B = 0$. This algorithm allows us to indicate the most contributing channel in a given area of an image. The algorithm was applied to 25 ortophotomaps obtained from Inspire 2 quadrocopter flights. The basic principle was to classify the max(B) and max(G) areas into white sediment (S.1) and max(R) to red sediment (S.2). In the area where separation of dominant color was difficult or impossible, the composite zone was determined. It should be noted that areas with low turbidity [<4 formazine nephelometric units (FNU)] for the parameter measured in the laboratory, shown as blue on the orthophotomap water surface and classified as max(B), were not considered for further analysis due to insufficient SSC [17]. Detailed information on the number of individual measurement points within a given sediment type is presented in Table II.

C. In Situ *Measurements*

To analyze the turbidity and SSC in the surface layer of water, water samples were collected at 20 evenly located points (Z1 - Z20) in the cove [see Fig. 1(c)]. Samples were stored in 1-L plastic bottles on the deck of a floating boat. During sampling, the turbidity (in FNU) of the surface water layer was measured (in the further analysis called T_F) using the optical sensor of the YSI EXO2 sonde (YSI, Inc., Yellow Springs, USA). For details see [13].

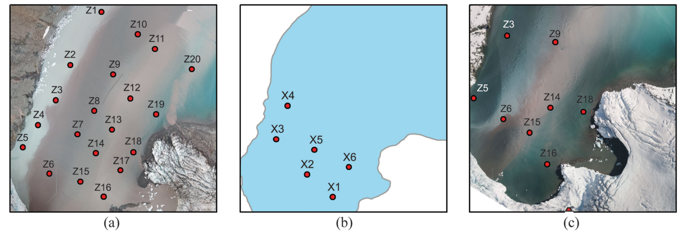

Fig. 2. Location of water sampling points for chemical composition analysis. (a) 06.01.2021, image taken on the same day. (b) 14.02.2020, no image. (c)12.01.2021, image taken on the same day. Z1-Z20, X1-X6 – sampling points.

D. Laboratory Measurements

Laboratory analyses were performed on half-liter samples. Initially, each 0.5-L water sample was remeasured (turbidity) in the dedicated YSI EXO2 measuring cylinder (in further analysis called T_{LAB}).

Turbidity is an indirect measurement that is influenced by many factors (type of particles, concentration, size, color). Therefore, it was decided to perform the turbidity measurements twice, which made it possible to obtain a turbidity value corresponding directly to measurements from the field (T_F) and directly related to the water samples analyzed in the laboratory (T_{LAB}).

Then, each sample was filtered using a vacuum pump, and the filters with the sediment were dried and weighed to obtain the SSC.

Another sequential step was sample measurement by using the LISST-200X particle size analyzer (Sequoia Scientific, Inc., Bellevue, WA) optical sonde, which is a submersible laser diffraction-based particle size analyzer designed to measure particle size and concentration.

From each 0.5-L sample, 12 mL were taken and poured into a small-volume test chamber of the LISST-200X particle size analyzer to measure the MPD (μm) for 20 s. According to guidelines, the measurement results in the first second were removed due to a possible measurement error. To calculate the MPD for each sample, the mean for each second of both samples was calculated, and then the result was averaged over the entire measurement time. It should be noted that in the case of samples with very high turbidity, due to the low transmittance, the device could not perform the measurement.

E. Chemical Composition Assessment

To determine the chemical composition of the suspended sediment, 14 surface water samples and 2 types of dried sediment were analyzed. Samples for analysis were collected on three different days with white and red suspensions on the surface of cove dried sediment from monitoring on 6.01.2021 [see Fig. 2(a)], and water samples were collected on 14.02.2020 and 12.01.2021 [see Fig. 2(b)-(c)].

The samples for analysis were selected to represent the diversity of the sediment on the surface of the cove as presented in Fig. 1(d). The dried sediment was collected after the filtration and drying process, previously described in Section II-D.

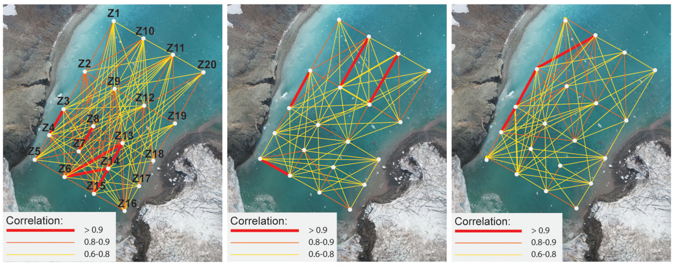

(a) (b) (c)

Fig. 3. Correlation maps. (a) Turbidity measured in filed (T_F). (b) Turbidity measured in laboratory (T_{LAB}). (c) SSC. Z1-Z20 – sampling points.

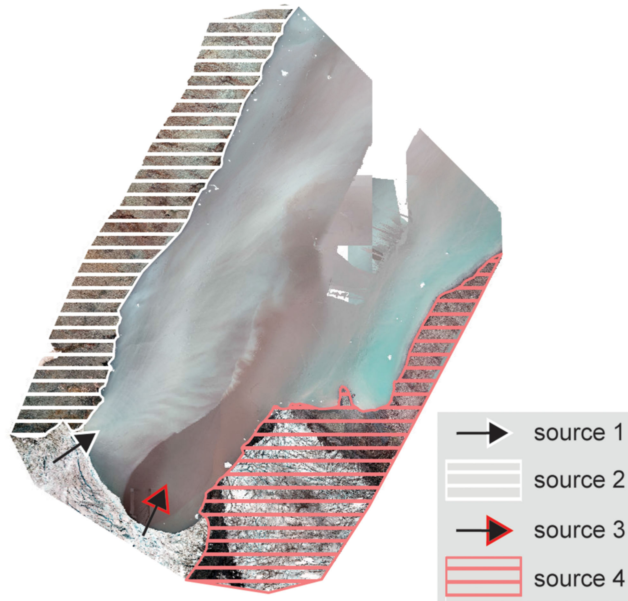

Fig. 4. Sources of sediment. Signs: arrow with white/red border – glacial flux with white/red suspension. A white/red patterned area – surface runoff area providing white/red sediment.

Based on the field observation of the spatial diversity of the suspension color and the color of the filtered sediment, two types of sediment were distinguished for chemical composition analysis: the sediment collected at points Z1, Z2, Z3, Z4, and Z5 was marked as S.1 (representation of white suspension), and the sediment designated S.2 represented the samples from the remaining points (red suspension representation) as illustrated in Fig. 2(a).

Water samples were tested for the amount of Fe, Ca, and Al, while the percentages of iron (Fe_2O), aluminum (Al_2O_3), silica (SiO_2), manganese (Mn_3O_4), calcium (CaO), magnesium (MgO), sodium (Na_2O), potassium (K_2O), phosphorus (P_2O), sulfur (SO_3), zinc (ZnO), copper (Cu), carbonates (CO_2), and total organic carbon (TOC) were determined in the dried sediment samples. The presence of almost all elements (except CO_2 and TOC) was determined using an inductively coupled plasma optical emission spectrometry method. This method quantitatively and qualitatively determined elements in a very wide range of concentrations, from 1 $n\cdot g\cdot L^{-1}$ to 1 $g\cdot L^{-1}$, both in liquid and solid samples, after being dissolved into a solution. The presence of CO_2 and TOC was determined via combustion infrared detection.

III. Results

A. *Sources of Sediment*

To indicate the resemblance of parameter changes at the sampling point, correlation maps of T_F, T_{LAB}, and SSC were created as shown in Fig. 3.

As presented in Fig. 3(a), the strongest correlation (>0.9) of T_F occurs between the pairs of points Z3–Z4, Z7–Z8, Z13–Z14, Z14–Z15, Z6–Z14, and Z6–Z13. A correlation of 0.8–0.9 occurs densely in the central part of the cove and the central part near the glacier terminus (points Z6, Z8, Z13, Z14, Z15) and moves to the left shore of the cove (points Z2, Z3). The weaker correlation of 0.6–0.8 occurs at the extreme points closest to the glacier, located on the right side of cove (Z5, Z16) and between the points farthest from the glacier front (Z1, Z10, Z11, Z20).

According to Fig. 3(b), the strongest T_{LAB} correlation occurs between pairs Z2–Z3, Z5–Z6, Z9–Z10, and Z11–Z12. A correlation of 0.8–0.9 is observed between the points closest to the glacier terminus (Z5–Z6, Z6–Z7, Z7–Z16, Z14–Z15, Z15–Z16) and near the left shore (Z1–Z2, Z3–Z4) combining points distant from the shore (Z1–Z10, Z2–Z9, Z2–Z10, Z3–Z10). A similar connection occurs in the center of the cove (Z8–Z13, Z13–Z12) and the points most distant from the glacier front on the right side of the cove (Z12–Z19, Z19–Z11, Z19–Z20). The least correlating points were located on the right side of the cove (Z17, Z18, Z19, Z20).

As shown in Fig. 3(c), the strongest correlation of SSC occurs only between points near the left bank (Z2–Z3, Z2–Z10, Z3–Z4). A correlation of 0.8–0.9 is most often also found near the left shore (Z1–Z2, Z1–Z9, Z1–Z10, Z2–Z9, Z3–Z10, Z3–Z9, Z4–Z5, Z4–Z9, Z4–Z10), descending toward the center of the cove (Z1–Z12, Z2–Z13, Z4–Z13, Z9–Z10, Z9–Z12, Z9–Z13, Z10–Z12, Z10–Z13, Z11–Z12, Z12–Z13), and the right shore far from the glacier (11–19, 12–19). Correlations also occur between points located close to the glacier (Z5–Z6, Z6–Z7, Z14–Z15, Z15–Z16). The least correlated points were located on the right side (Z17, Z18).

Based on the maps and their origins, four types of sediment sources as presented in Fig. 4 were defined.

1) Subglacial outflow on the left side of the cove – white sediment (S.1). A low correlation with points lying on the same line near the glacier face (Z15, Z16) and on the same line along the left bank (Z4, Z5) may indicate a different source. In the field, a visible glacial gate releases heavily turbid plumes of white color.
2) Surface run-off from the slope on the left side of the glacier – white sediment (S.1). This was based on a strong correlation between points on the same line (Z1, Z2, Z3, Z4) and a weaker correlation with point Z5. In the field, numerous gullies run down to the water.
3) Subglacial outflow on the right side of the glacier front – red sediment (S.2). This was based on the correlation

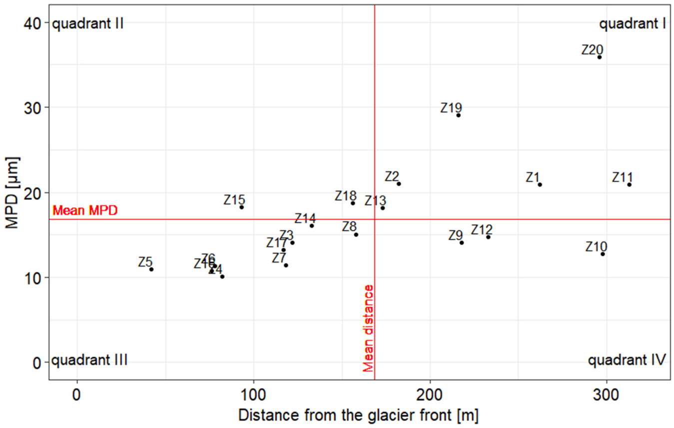

Fig. 5. Distribution of MPD depended on the distance from the glacier front. Z1-Z20 – sampling points of MPD on cove surface.

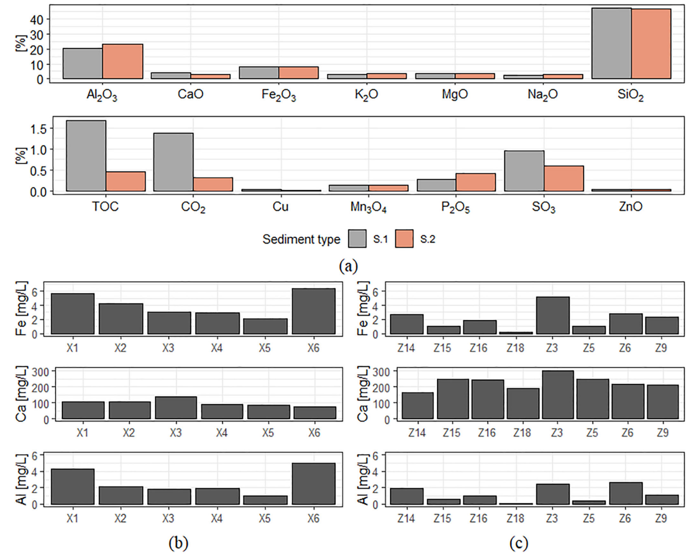

Fig. 6. Chemical compositional analysis results. (a) Dried sediment. (b) Water samples from February 14, 2020. (c) Water samples from January 12, 2021. Z3–Z18, X1–X6 – sampling points.

between points Z14, Z15 and Z16. In the field, numerous glacial gates can be seen from which red plumes flow.

4) Surface run-off from moraine on the right side of the glacier. This class was designated on the basis of correlation between points Z19 and Z20 and Z19 and Z11. Currently, as a result of the melting of the glacier, the run-off from the moraine also includes points Z17 and Z18. Sources 1 and 2 provide material from the Znosko Glacier geological formation, while sources 3 and 4 provide material from the Point Thomas Formation.

The variability in sediment sources was also investigated through particle size distribution analysis depending on the distance from the glacier front. Fig. 5 shows the distribution of MPD depending on the distance from the glacier front. Z1–Z20 – sampling points of MPD on cove surface. On this basis, the presence of several sources was demonstrated, including the presence of surface runoff on both sides of the cove. This result is evidenced by the presence of points in quadrant I – farthest from the glacier front, where the mean MPD is the highest. Points in quarter III are influenced by subglacial outflows – closest to the glacier, the finest particles. Points in quadrants II and IV are in the mixing zones. The exception may be point Z15, where the number of measurements made by LISST is reduced compared to that at other points due to the excessively high turbidity of the suspension at this location and insufficient transmittance – the obtained result may not be reliable.

For the analysis of the chemical composition of the two types of dry sediment, points from monitoring on 06.01.2020 were selected. Points Z1–Z5 represent sediment marked S.1, and the remaining points represent sediment S.2 as presented in Fig. 3(a). Both sediments are characterized by the same percentages of ZnO and Cu. S.1 has a higher percentage of Mn_3O_4, Fe_2O_3, SO_3, MgO, SiO_2, CO_2, CaO, and TOC than S.1. and S.2 has a higher percentage of P_2O_5, Na_2O, and Al_2O_3 than S.1. Fig. 6(a) shows the significant differences which occurred in the amount of TOC, CaO, SO_3, and P_2O_5 in relation to the total percentage of these elements in both groups.

The analysis of the chemical composition of surface seawater was conducted for white and red suspensions from 14.02.2020 to 12.01.2021. Total Ca, Al, and Fe content were analyzed. On the first measurement day, the highest amount of Ca was recorded at point X3 (140 mg/L), which was located on the left shore, close to the glacier terminus as presented in Fig. 6(b). The smallest amount of Ca was observed at point X6 (76.1 mg/L) on the right side of the cove. The highest amount of Fe was noted at points on the right side of the cove, with sites X1 and X6 exhibiting concentrations of 5.67 and 6.39 mg/L, respectively. The minimum Fe concentration was observed in the central part of the cove at point X5 (2.08 mg/L). The spatial distribution of Al refers to the spatial distribution of Fe, and the maximum values were noted at the same points X1 and X6 (4.31 and 5.04 mg/L, respectively). The lowest Fe concentration was recorded at point X5 (1.0 mg/L). On the second measurement day, the amount of Ca ranged from 166 to 301 mg/L; however, the maximum values were recorded at point Z3 on the left bank of the cove and the right side near the glacier terminus sites Z15 and Z16 as presented in Fig. 6(c). The Fe and Al content showed significant variability. The highest Fe values were observed at points within plumes – Z3 (5.15 mg/L), Z6 (2.80 mg/L), Z9 (2.34 mg/L), Z14 (2.67 mg/L), and Z16 (1.85 mg/L). The lowest Fe values were observed within blue water at sites Z5 (1.03 mg/L), Z15 (0.991 mg/L), and Z18 (0.236 mg/L), and the Al content at these points was also the lowest at 0.4, 0.59, and 0.14 mg/L. At other points, the Al content ranged from 1.03 to 1.92 mg/L.

Analysis of the MPD within a particular sediment type showed that the differences were not significant (p-value $= 0.08$) between white (S.1) and red (S.2) sediments. However, white sediment had a larger MPD and median than red sediment as shown in Fig. 7(a). Granulometric analysis showed that in the white sediment, the silt fraction reached 95% and the sandy fraction reached approximately 5%. On the other hand, in the red sediment, silt accounted for 98.6%, and sand accounted for 1.4% as illustrated in Fig. 7(b).

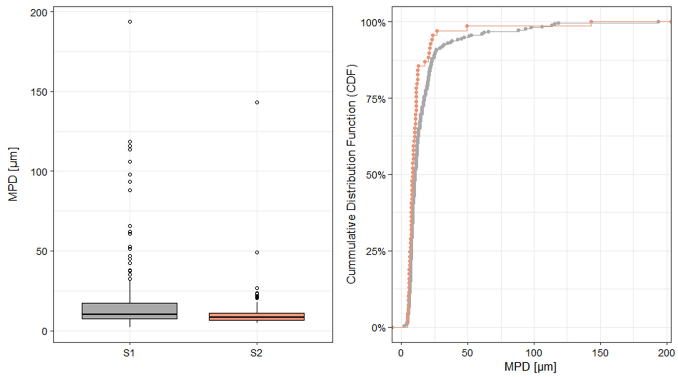

(a) (b)

Fig. 7. Granulometric analysis of both types of sediment. (a) Boxplot for MPD values of white (S.1) and red (S.2) suspension. (b) Cumulative curve of particle size distribution.

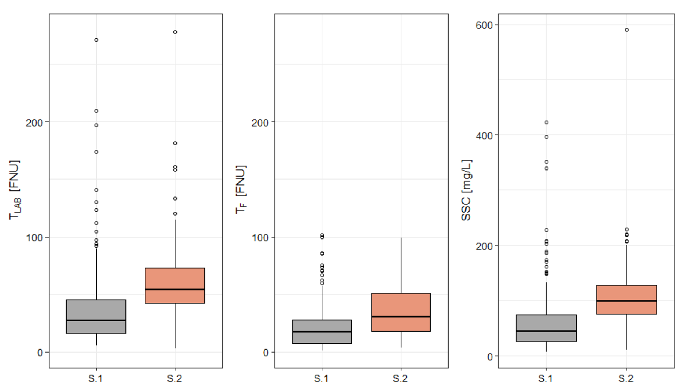

(a) (b) (c)

Fig. 8. Statistical analyses for individual parameters within sediment types (white – S.1, red – S.2): (a) Turbidity measured in laboratory (T_{LAB}). (b) Turbidity measured in field (T_F). (c) SSC.

The hypothesis of statistically significant differences between S.1 and S.2 for the three parameters T_{LAB}, T_F, and SSC was tested. The results presented in Fig. 8 show that differences between sediments for the three parameters were statistically significant. For the T_{LAB} parameter, the mean value for S.1 was 36.0, and that for S.2 was 62.7. The median values for T_{LAB} for S.1 and S.2 were 27.6 and 54.1, respectively. For T_F, the mean value for red sediment (S.2, 36.6) was 13.5 higher than that for white sediment (S.1). On the other hand, the median T_F was 30.6 for S.2 and was higher than that for S.1 by 13.0. The mean SSC for the red sediment was 110.2 and was higher than that for S.1 by 50, while the median for this parameter for the red sediment was 99 and was higher than that for S.1 by 55.

B. *Suspension Parameters Versus R_{RS}*

The next step in the analysis was to compare the parameter values obtained in individual types of sediments with the R_{RS} obtained in a given area.

To analyze the effect of sediment color on spectral reflectance, three transects were carried out on R_{RS} maps from 09.01.2020

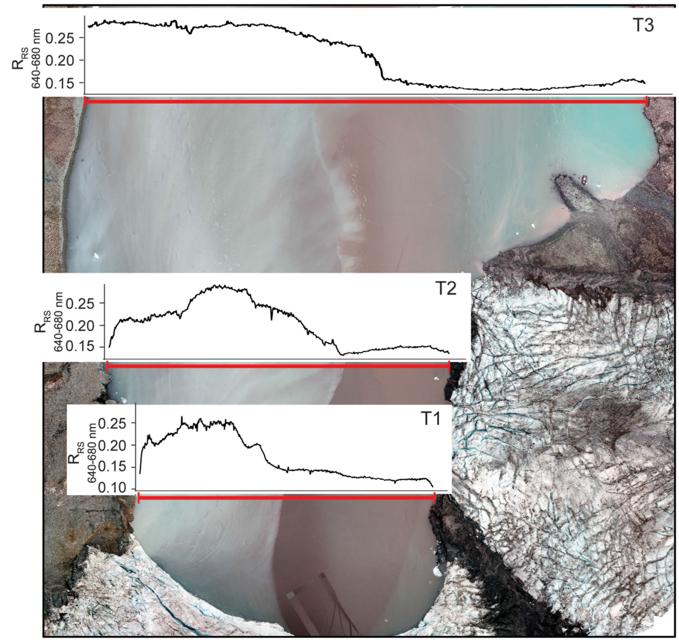

Fig. 9. Transects to analyze the effect of color on spectral reflectance. Image: orthophoto from 09.01.2020. Transect based on reflectance map obtained 09.01.2020.

with white (S.1) and red (S.2) sediment on the surface as illustrated in Fig. 9. In figure, results obtained only for red spectral band were presented to avoid redundancy. The transects were arranged in such a way that it was possible to register the spread of sediment along the cove. As a result of the analysis, there was also a visible change in the amount of reflectance in places of a clear change in the color of the sediment. In the case of the red sediment, the reflectance decreased by approximately 0.1 R_{RS} in each transect. As a result of the blurring of the boundary between the two sediments along with the distance from the glacier front, the boundary of the decrease in the amount of reflectance was also blurred. It is also worth noting that the spectral reflection within the white sediment was subject to greater fluctuations than that within the red sediment. Additionally, in the T3 transect, the spectral reflections within the red sediment and clear water were almost equal.

Fig. 10 shows linear regression plots between MPD and reflectance which indicate that the relationship is negative in all cases. The maximum correlation of parameters occurred in the NIR for the white sediment (S.1) ($R = -0.23$). The smallest correlation was in the NIR for the red sediment ($R = -0.096$). Spearman's rank correlation values presented in Table III were higher. For white sediment obtained values ranged from -0.29 to -0.38 and for red sediment ranged from -0.27 to -0.45.

As shown in Fig. 11, the correlation between the R_{RS} in each spectral band and the analyzed parameters (T_{LAB}, T_F, SSC) within the white sediment (S.1) was positive. Within the white sediment, the weakest correlations were obtained in the green spectral band for T_{LAB} ($R = 0.27$) and SSC ($R = 0.3$). In the remaining spectral bands, correlations were much higher and ranged from 0.52 to 0.69, with the highest correlation being achieved in the red spectral band with T_F, in NIR with SSC and

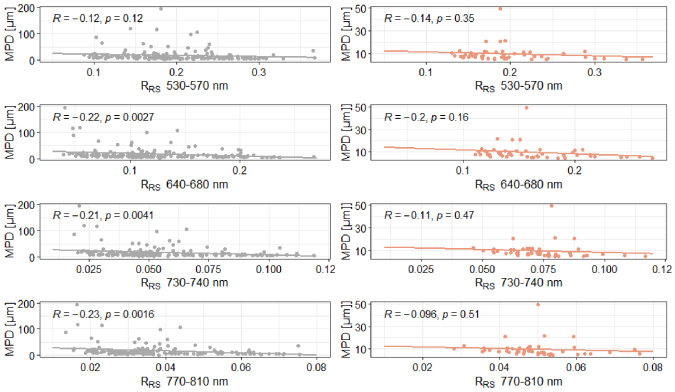

Fig. 10. Linear relationships between spectral bands and MPD. R and p – values for Pearson correlation coefficient.

TABLE III
SUMMARY OF SPEARMAN'S RANK CORRELATION COEFFICIENT VALUES BETWEEN MEASURED MPD OF TYPE OF SUSPENSION AND R_{RS}

	White sediment - S.1			
	R_{RS} 530-570 nm	R_{RS} 640-680 nm	R_{RS} 730-740 nm	R_{RS} 770-810 nm
MPD	-0.29	-0.38	-0.33	-0.35
	Red sediment - S.2			
	R_{RS} 530-570 nm	R_{RS} 640-680 nm	R_{RS} 730-740 nm	R_{RS} 770-810 nm
MPD	-0.27	-0.43	-0.43	-0.45

TABLE IV
SUMMARY OF SPEARMAN'S RANK CORRELATION COEFFICIENT VALUES BETWEEN MEASURED PROPERTIES (T_{LAB}, T_F, SSC) OF TYPE OF SUSPENSION AND R_{RS}

	White sediment - S.1			
	R_{RS} 530-570 nm	R_{RS} 640-680 nm	R_{RS} 730-740 nm	R_{RS} 770-810 nm
T_{LAB}	0.2680	0.6377	0.6213	0.6072
T_F	0.3398	0.6817	0.5492	0.4929
SSC	0.2724	0.7016	0.7315	0.6957
	Red sediment - S.2			
	R_{RS} 530-570 nm	R_{RS} 640-680 nm	R_{RS} 730-740 nm	R_{RS} 770-810 nm
T_{LAB}	-0.37390	-0.05072	0.12836	0.18349
T_F	-0.25048	0.00360	-0.13833	-0.08794
SSC	-0.37346	-0.10182	0.08263	0.12053

in RE with SSC. Maximum Spearman's rank correlation values for white suspension as presented in Table IV were obtained in red spectral band with SSC ($\rho = 0.7$) and RE spectral band with SSC ($\rho = 0.73$).

The relationship between the spectral reflectance and the water parameters within the red sediment (S.2) as shown in Fig. 11 was negative in 7 of 12 cases. In the green spectral bands, all parameters correlated negatively; in red, two parameters were negatively correlated; and in the RE and NIR bands, only T_F correlated negatively. The three strongest negative correlations were recorded in the green spectral band for SSC (R = −0.37), T_F (R = −0.19) and T_{LAB} (R = −0.36). The strongest positive correlation was in the NIR spectral band for T_{LAB} (R = 0.16) and SSC (R = 0.16). Obtained Spearman's rank correlation values were similar (see Table IV).

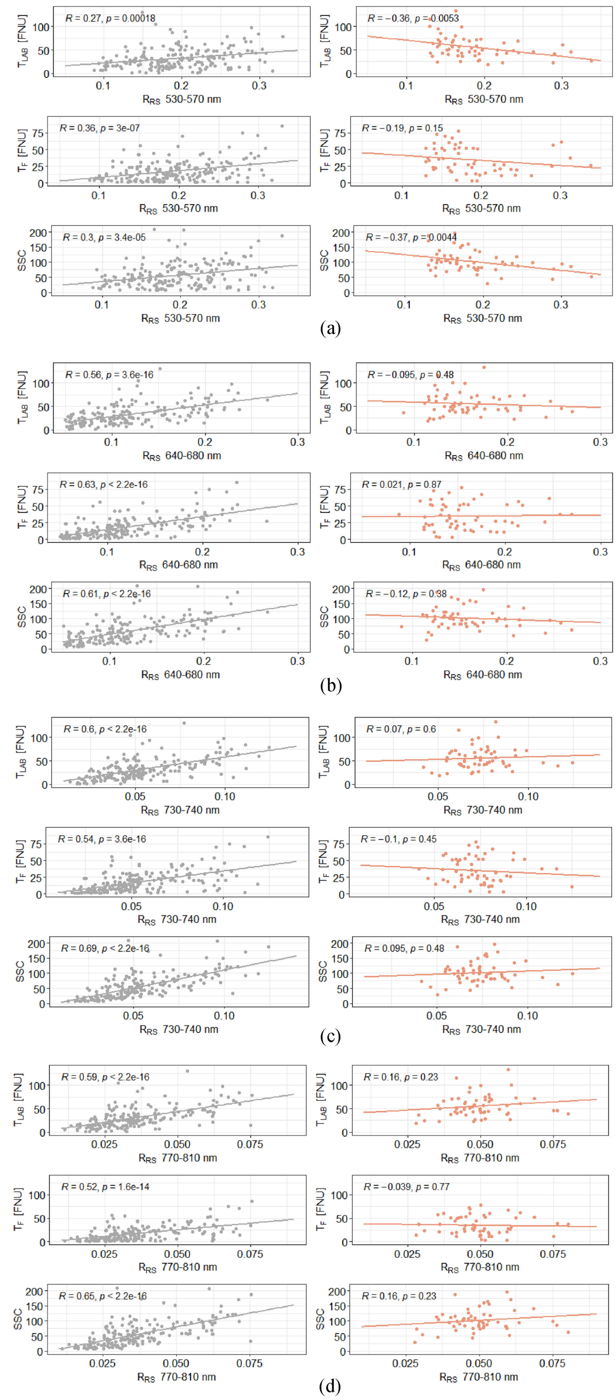

Fig. 11. Linear relationships between spectral bands and water parameters (T_{LAB}, T_F, SSC). (a) Green spectral band. (b) Red spectral band. (c) RE spectral band. (d) NIR spectral band. R and p – values for Pearson correlation coefficient.

IV. DISCUSSION

Within one glacier catchment area, there may be several sources of sediment [8]. Each of the sediment sources may be affected by other erosion and transport processes, which, in turn, will have an impact on the grain texture, including size and surface shape [18]. Determining the source area is also crucial in the process of determining the mineral and chemical composition of the sediment and is particularly important in glaciated mountain areas with different geological structures of the substrate, e.g., Svalbard, South Shetland Islands, Tierra del Fuego [19]–[21], where large ice surfaces such as glaciers, ice fields, and ice sheets erode the bed substrate, providing various sediments with meltwater. In the case of the Zalewski Glacier catchment, two source areas belonging to different geological groups were separated, which provided material to the cove in two ways – as a result of subglacial outflows and as a result of surface runoff. This result was confirmed by the different colors of the delivered sediment, as well as by the spatially differentiated SSC and turbidity [see Fig. 3(a)–(c)]. A strong argument supporting several sources of delivery is the spatial distribution of the particle size (see Fig. 5). The concentration of mixed-sized particles in the proximal zone indicates glacial flux. On the other hand, a high concentration of large particles in the distal location suggests the dominance of surface discharge at this point; otherwise, according to the general theory of glaciomarine sedimentation, very small particles should dominate in this zone and large particles should settle to the bottom of the cove [22]. When discussing the correlation of suspension parameters on the cove surface, the circulation issue should be taken into consideration. The matter of flow pattern and circulation in the cove near Zalewski Glacier has not yet been investigated due to the relatively young age of this cove. However, it is known that in fjord-shaped bays, the movement of the surface layer of water is mainly forced by the direction of local winds [23]. In Admiralty Bay, south-west winds prevail [24], which are parallel to the direction in which both coves at the Zalewski Glacier and the entire Ezcurra Inlet extend. Limited research on circulation in this area, both during significantly predominant W/S winds and during windless conditions (wind speed below 3 m/s), shows surface water run-off toward the central part of Admiralty Bay [25]. This is evident in satellite images that exhibit patterns of surface waters infused with sediment flowing along Ezcurra Inlet. This may suggest that the water movement caused by the wind within the cove affects the correlation of suspension parameters between individual points (the strongest correlation values occur in the direction parallel to the cove shore). However, it should be taken into account that the cove at Zalewski Glacier is located at the end of Ezcurra Inlet, in a place which, due to the proximity of the ice dome and peaks on both sides, is sheltered from strong gusts of winds. Therefore, the influence of the wind itself should not be overestimated. Robakiewicz and Rakusa-Suszczewski [26] also draw attention to the influence of tides on the hydrodynamic condition in Admiralty Bay. The tides in this area have a spectrum of approx. 1.7 m; however, this process has not yet been recognized within the cove nearby Zalewski Glacier, so it is not known how specifically it affects water movement on the surface.

Knowing that the color of the sediment strictly depends on its mineral and chemical composition [27], an attempt was made to determine the chemical composition of both types of sediment. First, in both types of sediment, silica predominates in the composition, which proves the clay structure of minerals with a similar specific gravity. This observation excludes a factor that could differentiate the two sediment types in terms of a different amount of reflected radiation [28]. According to Guimarães *et al.* [29], the main color-forming factors of the sediment are the content of TOC and the presence of various forms of iron. The effect of iron on the color of the sediment, regardless of its form, is not significant in this case due to the similar percentage of this element in both types of sediments. Significant differences in the chemical composition of dry sediment occurred in the percentage of TOC, carbonates, sulfur, and phosphorus. Despite the difference in TOC content between the two types of sediment, their percentage is still very small [30]. However, knowing that TOC gives a dark, coffee coloration, it can be concluded that its content in the white sediment is not a color-forming dominant factor [31]. Phosphorus itself does not directly affect the color; however, its increased presence can affect algal blooms [32], and this can cause coloration; however, this factor is not considered in this case. Similarly, the determining factor, with such a percentage, is not the sulfur content. The content of carbonates, which have a white tint [33], may have the greatest influence on color. The presence of these compounds in polar waters has already been observed [34]. These compounds, in the form of insoluble sediment, enter nearby coves as a result of the erosion of the substrate forming the catchment area of the glacier and as a result of surface runoff, and their presence in the marine environment affects the surface water chemistry [34]. Analysis of the chemical composition of the surface layer of water over two days showed that the presence of basic chemical elements may change dynamically with the spread of plumes, which is influenced by the origin of supply and quantity of melted water, stratification in the fjord, and shape of the glacier front [35], [36]. In addition, the chemical or mineral composition of the material that enters the cove as a result of direct runoff from a glacier or as a result of indirect runoff may differ from each other because surface discharge can be additionally enriched [7], which means that even within one source area, not only grain size but also chemical composition may differ, causing the formation of different zones of increased surface stratification and light attenuation by terrestrial lithogenic material contained in the meltwater (such as silicates, carbonates, clay), which, in turn, reduce productivity in fjords [37]. The effect of the chemical composition of sediment on reflectance has already been described by Bhargava and Mariam [38]. It has been proven that some chemical compounds contained in the sediment cause a negative correlation between these parameters. The presence of chemical compounds in the sediment, which will give a lighter color to the particles, will cause an increased reflection of electromagnetic radiation than the darker ones, which are characterized by greater absorbance of radiation [9]. Conversely, the darker color of the water reduces the flux of energy reaching the sensor because more of the sun's energy is absorbed in the water [10].

The reflection of radiation increases with a decrease in particle size, resulting from the reduction in the scattering surface and the increased number of particles and, as a result, a greater number of reflections [39], [40]. By analyzing the R_{RS} relationship plots in all spectral bands with MPD for each type of sediment separately as presented in Fig. 11, such a phenomenon was also observed – the relationship between these two parameters was slightly negative. However, analysis of the particle size of the white (S.1) and red (S.2) sediments showed that the mean and median MPD for the white sediment was greater than that for the red sediment. In the white sediment, the sand fraction is characterized by a higher percentage than in the red sediment. It was, therefore, expected that the white sediment would reflect less radiation than the red sediment, but as shown in Fig. 10, an opposite phenomenon was observed. Our observations contradict the results obtained by Choubey [28] that the increased proportion of the finer fraction could increase the reflection, despite the darker color of the grains. This observation points to the fact that in the relationship between the $\mathrm{R_{RS}}$ and sediment parameters, particle size does not play a key role, at least in the case of a comparative analysis of different colored sediments. Comparable results were obtained by Kabir and Ahmari [9], which indicate that the amount of reflected radiation is not determined by the sediment particle size but by different SSCs or colors. Similar conclusions were also reached in the [39] studies, in which it was found that with the same concentration and particle size of different types of sediment, different reflection curves were obtained, indicating that the main determinant may be differences in their properties and characteristics.

Both SSC and turbidity are parameters that directly affect the amount of reflectance, and their relationship is most often described as a positive linear correlation or nonlinear regression [1], [2], [9]. Knowing that the delivered sediment comes from different sources, the differences in these parameters between the sediment types were initially analyzed, indicating that the red sediment is characterized by higher median and mean $\mathrm{T_{LAB}}$, $\mathrm{T_{F,}}$ and SSC values than the white sediment. Analysis of the linear relationships between SSC and $\mathrm{R_{RS}}$ showed that the red sediment negatively correlated with two spectral bands, and a reduction in the negative correlation occurred with the elongation of the electromagnetic wave. The white sediment correlated positively with the SSC in all spectral bands, and the weakest correlation was reached in the green bands. Some studies, focusing their attention on the relationship between SSC and $\mathrm{R_{RS}}$, indicate the influence of the type of sediment, including color, on this relationship [9], [41]. The results of Kabir and Ahmari [9] found that the color of the sediment may be an important factor affecting the relationship between reflection and concentration. Light brown sediment reflects 7.33% more radiation than dark gray sediment. However, in linear regression models between these parameters, a difference in R^2 coefficients of 0.02 was obtained when analyzing dark brown and dark gray sediments. In the experiment conducted by Novo *et al.* [11], it was also suggested that white sediment reflects significantly more radiation than red sediment regardless of the concentration of the suspension, but importantly, in this experiment, this effect was also due to the difference in particle size between different types of sediment. Nonetheless, for both types of sediment, a strong positive correlation was obtained in almost the entire spectrum of radiation (except for the blue spectral band). The studies conclude that the type of sediment may affect the relationship between SSC and reflection, resulting in a decrease or increase in this relationship; however, the results presented in this article indicate that the dominant color may be a key factor in this relationship, causing its complete reversal. The SSC parameter itself may not be sufficient in creating models, assuming automatically/in advance a positive relationship between SSC and reflectance, particularly in areas that may provide nonuniform material temporarily, for example, after storms, or permanently [9].

Similar results were also obtained from observations of the relationship between $\mathrm{T_{LAB}}$, $\mathrm{T_F}$, and $\mathrm{R_{RS}}$. A negative relationship in three spectral bands was obtained between $\mathrm{T_F}$ and $\mathrm{R_{RS}}$ for red suspension, while the relationship between $\mathrm{T_{LAB}}$ and $\mathrm{R_{RS}}$ obtained a negative correlation in the green and red spectral band. The correlation of these parameters for the white suspension, similar to SSC, was positive in all cases. A similar study by Bhargava and Mariam [39] indicates that the magnitude of reflection varies for different types of sediments of different turbidities, but the relationship between turbidity and reflectance, regardless of the color of the sediment, is strongly positive. This observation points to the insufficiency of the assumption that turbidity is in a direct relationship to reflection and increases with it. Turbidity, as an optical parameter measuring the amount of scattered light, also depends on the color of the grains because the more intense the color is, the more light is absorbed and the turbidity is greater than in reality [42].

The relationship between the parameters of the suspension and $\mathrm{R_{RS}}$ is highly individualized, and whether the color, concentration, or particle size will have a greater impact on the reflectance depends on the local conditions, which is confirmed by the analysis carried out in this article and previously quoted studies. Kabir and Ahmari [9] mentioned that previously created empirical models based on local data may not be effective under global conditions because the relationship between reflectance and SSC is affected by the particle size distribution and sediment mineralogy. However, it could be said that creating universal algorithms based solely on turbidity or concentration values, without making adjustments that would normalize the variability in particle size or chemical composition within one catchment area, remains universal only in theory. It was confirmed that the diversity of sediment can be significant even within one glacial catchment. This means that the material differs not only in the chemical composition resulting from the different petrographic compositions between the source areas but also in the size of grains within one area. The suspension types can differ significantly in the size of the parameters, which, even in the case of homogeneous sediment, may be problematic for algorithms that have been validated for a different sediment type or do not take into account all the variables. In addition, this article shows that the color of the sediment, which is related to the chemical composition, has a large impact on the relationship between the parameters of the suspension and reflectance and may also be a source of errors in algorithms that are not color-normalized.

V. Conclusion

The following points summarize our findings.

1) In this study, we confirmed based on multivariate analyses that the sediment to the cove in front of the Zalewski Glacier comes from two geologically different source areas. Additionally, each of these areas provides sediment in two ways: surface runoff and glacial runoff.

2) Two types of sediment on the cove surface were distinguished. Analysis of the chemical composition showed that both types of sediment are derived from silicate rocks and that the two sediments significantly differ in carbonates, TOC, sulfur, and phosphorus contents. Based on the literature, it was determined that the color difference may result from an increased number of carbonates in the white sediment (S.1).
3) Analysis of surface water samples for the quantitative presence of basic elements showed that their content on the surface may vary significantly with the formation and spread of plumes and with the activity of sea currents in the cove.
4) The white sediment (S.1) was characterized by a larger MPD than the red sediment (S.2) and by a greater percentage of the sand fraction. In both types of sediment, the size of the reflection decreased with increasing particle size. However, the comparative analysis did not show that sediment with a larger particle diameter (white sediment) reflected less radiation than that with small particle diameter.
5) The white sediment suspension (S.1) had lower mean $\mathrm{T_{LAB}}$, $\mathrm{T_F}$, and SSC values than the red suspension (S.2), by approximately 26.6 FNU, 13.5 FNU, 50 mg/L, respectively.
6) The relationship between the parameters and the $\mathrm{R_{RS}}$ showed that all parameters for the white sediment strongly positively correlated with the $\mathrm{R_{RS}}$, except for the green spectral band, in which the correlation values were weakest. For the red sediment, the relationship between the $\mathrm{R_{RS}}$ and the three parameters often showed a negative or positive correlation close to zero. This result proved that the color of sediment is crucial in studying the relationship between spectral reflectance and suspension parameters and should not be ignored.
7) Analysis showed that the color of the suspension can be a key factor in determining the dependence of the suspension parameters and the reflection.

Acknowledgment

The authors appreciate the support provided by the Arctowski Polish Antarctic Station. The authors are particularly grateful to the members of the 44th Polish Expeditions to King George Island. Special thanks to ESRI for providing the ArcGIS Advanced 10.8.1 to Kornelia Wójcik-Długoborska, which helped complete most analyses.

References

[1] A. I. Dogliotti, K. G. Ruddick, B. Nechad, D. Doxaran, and E. Knaeps, “A single algorithm to retrieve turbidity from remotely-sensed data in all coastal and estuarine waters,” *Remote Sens. Environ.*, vol. 156, pp. 157–168, 2015.

[2] K. M. Schild, R. L. Hawley, J. W. Chipman, and D. I. Benn, “Quantifying suspended sediment concentration in subglacial sediment plumes discharging from two Svalbard tidewater glaciers using Landsat-8 and in situ measurements,” *Int. J. Remote Sens.*, vol. 38, no. 23, pp. 6865–6881, 2017.

[3] G. Zheng and P. M. DiGiacomo, “Uncertainties and applications of satellite-derived coastal water quality products,” *Prog. Oceanogr.*, vol. 159, pp. 45–72, 2017.

[4] I. Caballero, G. Navarro, and J. Ruiz, “Multi-platform assessment of turbidity plumes during dredging operations in a major estuarine system,” *Int. J. Appl. Earth Observ. Geoinf.*, vol. 68, pp. 31–41, 2018.

[5] M. Rückamp, M. Braun, S. Suckro, and N. Blindow, “Observed glacial changes on the King George Island ice cap, Antarctica, in the last decade,” *Glob. Planet. Change*, vol. 79, no. 1/2, pp. 99–109, 2011.

[6] C. L. Simões, K. K. Rosa, J. C. Simões, R. Vieira, R. M. Costa, and A. B. Silva, “Recent changes in two outlet glaciers in the Antarctic Peninsula using multi-temporal Landsat and Sentinel-1 data,” *Geocarto Int.*, vol. 35, no. 11, pp. 1233–1244, 2020.

[7] A. Fransson *et al.*, “Effect of glacial drainage water on the CO 2 system and ocean acidification state in an Arctic tidewater-glacier fjord during two contrasting years,” *J. Geophys. Res., Oceans*, vol. 120, no. 4, pp. 2413–2429, 2015.

[8] A. Matmon, P. J. Haeussler, and A. Team, “Sediment sources and transport by the Kahiltna Glacier and other catchments along the south side of the Alaska Range, Alaska,” *Geosphere*, vol. 16, no. 3, pp. 787–805, 2020.

[9] S. M. I. Kabir and H. Ahmari, “Evaluating the effect of sediment color on water radiance and suspended sediment concentration using digital imagery,” *J. Hydrol.*, vol. 589, 2020, Art. no. 125189.

[10] G. K. Moore, “Satellite remote sensing of water turbidity,” *Hydrological Sci. J.*, vol. 25, no. 4, pp. 407–421, 1980.

[11] E. M. M. Novo, J. D. Hansom, and P. J. Curran, “The effect of sediment type on the relationship between reflectance and suspended sediment concentration,” *Remote Sens.*, vol. 10, no. 7, pp. 1283–1289, 1989.

[12] K. A. Wójcik, R. J. Bialik, M. Osińska, and M. Figielski, “Investigation of Sediment-Rich Glacial Meltwater plumes using a high-resolution multispectral sensor mounted on an unmanned aerial vehicle,” *Water*, vol. 11, no. 11, 2019, Art. no. 2405.

[13] M. Osińska, R. J. Bialik, and K. A. Wójcik-Długoborska, “Interrelation of quality parameters of surface waters in five tidewater glacier coves of King George Island, Antarctica,” *Sci. Total Environ.*, vol. 771, 2021, Art. no. 144780.

[14] M. Majdański *et al.*, “3D seismic model of the uppermost crust of the Admiralty Bay area, King George Island, West Antarctica,” *Polish Polar Res.*, vol. 29, no. 4, pp. 303–318, 2008.

[15] K. Birkenmajer, “Mesozoic and Cenozoic stratigraphic units in parts of the South Shetland Islands and Northern Antarctic Peninsula (as used by the Polish Antarctic Programmes),” *Studia Geologica Polonica*, vol. 118, pp. 5–188, 2001.

[16] M. A. Hussain and A. S. Akbari, “Max-RGB based colour constancy using the sub-blocks of the image,” in *Proc. 9th Int. Conf. Develop. eSystems Eng.*, 2016, pp. 289–294.

[17] World Health Organization, “Water quality and health-review of turbidity: Information for regulators and water suppliers,” 2017.

[18] A. Karczewski, G. Rachlewicz, and W. Szczuciński, “Sediment texture in contemporary glacial environment–examples from Hansbreen, southern Spitsbergen,” *Geologos*, vol. 6, pp. 111–131, 2003.

[19] J. L. Smellie, R. Pankhurst, M. R. A. Thomson, and R. E. S. Davies, “The geology of the south shetland islands: VI. Stratigraphy, geochemistry and evolution,” British Antarctic Survey Scientific Reports, 87, 1984.

[20] W. B. Harland *et al.*, *The Geology of Svalbard*. London, U.K.: Geological Society, 1997.

[21] R. D. Acevedo, *Geological Resources of Tierra Del Fuego*. Berlin, Germany: Springer, 2021.

[22] K. Licht, “Glaciomarine Sediments,” in *Encyclopedia of Paleoclimatology and Ancient Environments. Encyclopedia of Earth Sciences Series*, V. Gornitz, Ed. Dordrecht, The Netherlands: Springer, 2009.

[23] A. Stigebrandt, “Hydrodynamics and circulation of Fjords,” in *Encyclopedia of Lakes and Reservoirs. Encyclopedia of Earth Sciences Series*, L. Bengtsson, R. W. Herschy, and R. W. Fairbridge Eds. Dordrecht, Netherlands: Springer, 2012.

[24] J. Plenzler, T. Budzik, D. Puczko, and R. J. Bialik, “Climatic conditions at Arctowski station (King George Island, West Antarctica) in 2013-2017 against the background of regional changes,” *Polish Polar Res.*, vol. 40, no. 1, pp. 1–27, 2019.

[25] Z. Pruszak, “Currents circulation in the waters of Admiralty Bay (region of Arctowski Station on King George Island),” *Polish Polar Res.*, vol. 1, no. 1, pp. 55–74, 1980.

[26] M. Robakiewicz and S. Rakusa-Suszczewski, “Application of 3D circulation model to Admiralty Bay, King George Island, Antarctica,” *Polish Polar Res.*, vol. 20, no. 1, pp. 43–58, 1999.

[27] M. Debret *et al.*, "Spectrocolorimetric interpretation of sedimentary dynamics: The new "Q7/4 diagram," *Earth Sci. Rev.*, vol. 109, pp. 1–19, 2011.

[28] V. K. Choubey, "The effect of properties of sediment type on the relationship between suspended sediment concentration and radiance," *Hydrological Sci. J.*, vol. 39, no. 5, pp. 459–470, 1994.

[29] J. T. F. Guimarães, M. C. L. Cohen, M. C. França, A. K. T. D. Silva, and S. F. S. Rodrigues, "Mineralogical and geochemical influences on sediment color of Amazon wetlands analyzed by visible spectrophotometry," *Acta Amazonica*, vol. 43, pp. 331–342, 2013.

[30] P. K. Shrivastava, A. Dharwadkar, R. Asthana, S. K. Roy, A. K. Swain, and M. J. Beg, "The sediment properties of glacial diamicts from the Jutulsessen area of Gjelsvikfjella, East Antarctica: A reflection of source materials and regional climate," *Polar Sci.*, vol. 8, no. 3, pp. 264–282, 2014.

[31] S. Löfgren, M. Forsius, and T. Andersen, "Climate induced water color increase in Nordic lakes and streams due to humus," Nordic Council of Ministers, Brochure, Copenhagen, Denmark, vol. 12, 2003.

[32] W. W. Walker, Jr., and K. E. Havens, "Relating algal bloom frequencies to phosphorus concentrations in lake Okeechobee," *Lake Reservoir Manage.*, vol. 11, no. 1, pp. 77–83, 1995.

[33] Y. H. Kim, G. B. Kim, S. G. Choi, and C. S. Kim, "SWIR application for the identification of high-grade limestones from the Upper Pungchon formation," *Econ. Environ. Geol.*, vol. 49, no. 5, pp. 335–347, 2016.

[34] A. Fransson *et al.*, "Influence of glacial water and carbonate minerals on wintertime sea-ice biogeochemistry and the CO2 system in an Arctic fjord in Svalbard," *Ann. Glaciol.*, vol. 61, no. 83, pp. 320–340, 2020.

[35] E. D. Andrés, D. A. Slater, F. Straneo, J. Otero, S. Das, and F. Navarro, "Surface emergence of glacial plumes determined by fjord stratification," *Cryosphere*, vol. 14, no. 6, pp. 1951–1969, 2020.

[36] D. Carroll *et al.*, "The impact of glacier geometry on meltwater plume structure and submarine melt in Greenland fjords," *Geophys. Res. Lett.*, vol. 43, no. 18, pp. 9739–9748, 2016.

[37] M. Seifert *et al.*, "Influence of glacial meltwater on summer biogeochemical cycles in Scoresby Sund, East Greenland," *Front. Mar. Sci.*, vol. 6, 2019, Art. no. 412.

[38] D. S. Bhargava and D. W. Mariam, "The effect of variation in suspended sediment properties on reflectance measurements," *J. Indian Soc. Remote Sens.*, vol. 20, no. 2, pp. 139–152, 1992.

[39] D. S. Bhargava and D. W. Mariam, "Spectral reflectance relationships to turbidity generated by different clay materials," *Photogrammetric Eng. Remote Sens.*, vol. 56, no. 2, pp. 225–229, 1990.

[40] T. L. Myers, C. S. Brauer, Y. F. Su, T. A. Blake, T. J. Johnson, and R. L. Richardson, "The influence of particle size on infrared reflectance spectra," *Proc. SPIE*, vol. 9088, 2014, Art. no. 908809.

[41] H. G. Gebreslassie, A. M. Melesse, K. Bishop, and A. G. Gebremariam, "Linear spectral unmixing algorithm for modelling suspended sediment concentration of flash floods, upper Tekeze River, Ethiopia," *Int. J. Sediment Res.*, vol. 35, no. 1, pp. 79–90, 2020.

[42] Optek 2021, 2021, Accessed: Dec. 15, 2021. [Online]. Available: https://www.optek.com/en/turbidity-basics.asp

Kornelia Anna Wójcik-Długoborska received the B.Sc. degree in geography in 2016 and M.Sc. degree in environmental geoinformation in 2018 from the Nicolas Copernicus University in Toruń, Poland. She is currently working toward the Ph.D. degree with the Department of Antarctic Biology, Institute of Biochemistry and Biophysics, Polish Academy of Sciences.

Her research is focused on remote sensing of polar regions.

Maria Osińska received the first M.Sc. degree in international relations from the Jagiellonian University, Kraków, Poland, in 2013, and the second M.Sc. degree in physical oceanography from the University of Gdańsk, Poland, in 2020. She is currently working toward the Ph.D. degree in physical oceanography from the Institute of Oceanography, University of Gdańsk.

Her research interests include ocean dynamics, numerical modelling, and spatio-temporal data analysis.

Robert Józef Bialik received the B.Sc. degree in mathematics from the Pomeranian University, Słupsk, Poland, in 2006, the M.Sc. degree in physical oceanography from the University of Gdańsk, Poland, in 2004, and the Ph.D. degree in geophysics from the Institute of Geophysics, Polish Academy of Sciences, Warsaw, Poland, in 2010.

He is currently the Head of Department of Antarctic Biology with the Institute of Biochemistry and Biophysics, Polish Academy of Sciences. His research interests include use of remote sensing in monitoring Antarctic environment and numerical modeling of bedload sediment transport.